ISSN 1063-7834, Physics of the Solid State, 2021. © Pleiades Publishing, Ltd., 2021.
Russian Text © The Author(s), 2021, published in Fizika Tverdogo Tela, 2021, Vol. 63, No. 7, pp. 881–887.

MAGNETISM

Change in the Direction of the Easy Magnetization Axis of Arrays of Segmented Ni/Cu Nanowires with Increasing Ni Segment Length

A. A. Mistonov[a], I. S. Dubitskiy[b, *], A. H. A. Elmekawy[a, c], E. G. Iashina[b], S. V. Sotnichuk[a, d], K. S. Napolskii[d, e], and D. Menzel[f]

[a] *Saint Petersburg State University (SPbU), St. Petersburg, 199034 Russia*
[b] *Petersburg Nuclear Physics Institute named by B.P. Konstantinov of National Research Centre "Kurchatov Institute," Gatchina, Leningrad oblast, 188300 Russia*
[c] *Cyclotron Project, Nuclear Research Center, Atomic Energy Authority, Cairo, 13759 Egypt*
[d] *Moscow State University, Moscow, 119992 Russia*
[e] *Moscow Institute of Physics and Technology (National Research University), Dolgoprudny, Moscow oblast, 141701 Russia*
[f] *Technical University of Braunschweig, Institute for Condensed Matter Physics, Braunschweig, 38106 Germany*
**e-mail: ilya.dubitskiy@mail.ru*

Received November 2, 2020; revised February 2, 2021; accepted February 2, 2021

Abstract—Arrays of ordered segmented nanowires, which are ferromagnetic regions separated by non-magnetic inserts, are considered as a promising material for three-dimensional information storage systems. However, the presence of a large number of competing interactions significantly complicates the description of the magnetic behavior of such systems. In this paper, the effect of the segment length on the integral magnetic properties of Ni/Cu wires arrays is investigated. It is shown that the coercivity increases with an increase in the length of the magnetic segment for both the longitudinal and transverse directions of the long axis of the wires relative to the external magnetic field. A change in the direction of the easy magnetization axis was found with the ratio of the Ni segment length to the diameter in the range from 10 to 15.

Keywords: segmented nanowires, arrays of nanowires, micromagnetism, interaction of nanowires
DOI: 10.1134/S1063783421070179

1. INTRODUCTION

The development of methods for the synthesis of magnetic nanostructures in recent years has led to the possibility of creating systems with specified geometric parameters [1]. Significant progress in understanding the magnetic states of individual nano-objects (cubes, disks, pyramids) [2–4] has made it possible to proceed to the study of ensembles of particles [5, 6] and porous ordered structures [7, 8].

However, most of the systems currently being studied are consisted of objects ordered on a plane. Apparently, further progress will be associated with the study of three-dimensional ordered systems. There are two main groups of methods used for the synthesis of such structures: lithography [9] and techniques based on the effect of self-ordering of particles [10, 11]. Lithographic methods make it possible to control the geometric characteristics of the synthesized systems with high precision. As examples of objects obtained using this technique, one can single out a truncated icosahedron [9], a nanospiral [12], and an ordered lattice of nanowires [13]. The self-assembly technology is easier to use and allows the fabrication of samples of a larger area, however, direct control of the geometric parameters of the system is difficult. Nevertheless, using this method, the highly ordered three-dimensional periodic structures were successfully obtained: artificial opals [14] and inverse opals [15–17], mesocrystals [18, 19], and gyroids [20].

One of the most interesting manifestations of the self-ordering effect is observed in the preparation of porous films of anodic aluminum oxide (AAO) [21]. The structures with hexagonal pore ordering formed as a result of metal anodization can be used as a template for the synthesis of arrays of magnetic nanowires [22]. Improvement of this technology made it possible to obtain well-ordered arrays of nanowires and to ensure the reproducibility of experimental results, which led to an expansion of the range of possible applications of these systems [23]. Nanowires can be used in medicine to destroy cells using hyperthermia or mechanical vibrations [24, 25]; they can be used to fabricate waveguides and magnonic crystals for the needs of magnonics [26, 27]; due to the large magnetic

anisotropy, nanowires can be used to create permanent magnets [28] or needles for quantitative magnetic force microscopy [29].

The next step is to move to three-dimensionally ordered arrays of segmented nanowires. They can be obtained by sequential deposition of magnetic and non-magnetic materials, such as nickel and copper, into the pores of the template [30]. The interest in these systems is primarily due to the possibility of using such nanowires in spintronics [31] and superdense information recording [32]. At the same time, the distribution of magnetization in the arrays of segmented nanowires is nontrivial due to the long-range nature of the interaction between the nanowires [33]. In addition, the magnetic structure of nanowires significantly depends on their geometric characteristics [34]. In particular, by changing the length of the nonmagnetic segment, it is possible to modify the magnitude of the interaction in the system [35, 36]. An even richer picture of magnetic states can be obtained by varying the length of the ferromagnetic segments. In this case, not only the magnitude, but also the very nature of the interaction can change, since at a certain critical length of the ferromagnetic segment, the easy magnetization axis must change its direction. The first results obtained for small segments (up to 140 nm) indicate the possibility of antiferromagnetic ordering of magnetic moments [37]. This work is devoted to the study of this phenomenon in an array of segmented Ni/Cu nanowires with a nickel segment length from 140 nm to 1 μm.

2. SAMPLES

The arrays of segmented Ni/Cu nanowires (Fig. 1) were formed using the method of template electrodeposition into porous films of AAO. To obtain porous templates, a two-stage procedure of anodizing aluminum in 0.3 mol $H_2C_2O_4$ at a constant voltage of 40 V and a temperature of 0°C was used, which was described in detail elsewhere [38—41]. This two-stage technique leads to the formation of a highly ordered AAO structure with a hexagonal arrangement of pores in the plane of the film. The thickness of the oxide layer formed during the first and second stages was 10 and 35 μm, respectively. Etching of the AAO barrier layer was carried out in a solution of 3 mol H_3PO_4, while controlling the moment of pore opening and their further etching to a pore diameter of ~50 nm. At the last stage, a 200 nm thick gold layer was deposited on the bottom of the AAO template using magnetron sputtering on a Quorum Technologies Q 150T ES setup.

The electrodeposition of Ni nanowires was carried out at room temperature in a three-electrode cell of an electrolyte simultaneously containing copper and nickel ions. A porous AAO film with a sputtered current collector was used as a working electrode; a Pt wire served as an auxiliary electrode; a saturated (KCl) Ag/AgCl electrode connected to the cell through a Luggin—Haber capillary was used as a reference electrode. In this study, the following electrolyte composition was used: 0.005 mol $CuSO_4$, 0.5 mol $NiSO_4$, and 0.6 mol H_3BO_3. The deposition potential of Cu was −0.4 V, Ni was deposited at −1.0 V. It should be noted that under these conditions, metallic precipitates are formed containing both metals simultaneously: at a copper deposition potential ($E_d = -0.4$ V), the precipitate can contain up to 12% Ni, and at the nickel deposition potential ($E_d = -1.0$ V) — up to 3% Cu [42]. To increase the convective mass transfer of metal ions in the electrolyte solution, the solution was circulated using a Heidolph PD5006 peristaltic pump with a pumping rate of 0.5 L/min. The lengths of the copper and nickel segments were controlled coulometrically. As a result, three arrays of segmented nanowires with a nickel segment length of 140, 300, and 1000 nm were synthesized; the length of the copper segments was the same and amounted to 25 nm. The nanowires in each sample contained 10 repeated Ni/Cu fragments.

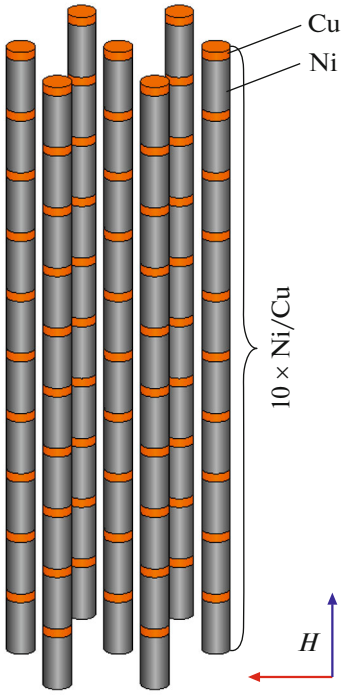

Fig. 1. Schematic representation of an array of segmented nanowires.

The surface morphology and cleavage of nanowire arrays in the AAO matrix were studied by scanning electron microscopy (SEM) using a Zeiss AURIGA Laser microscope (Research Park—Saint Petersburg State University) and Carl Zeiss Vision 40 (Kurnakov Institute of General and Inorganic Chemistry of the Russian Academy of Sciences). Since the contrast between the nickel and copper sections is too small,

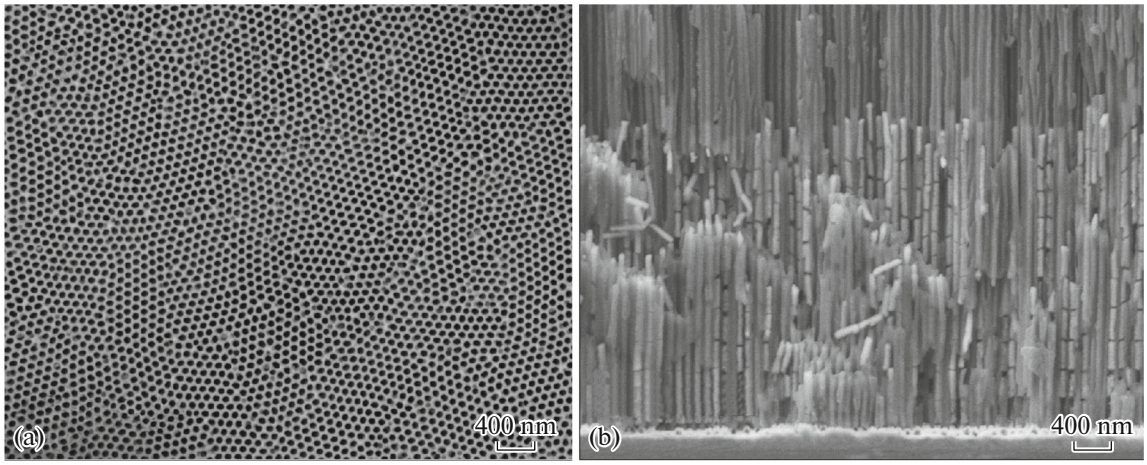

Fig. 2. SEM images of the surface (a) and side (b) of a nanocomposite containing nanowires with a magnetic segment length of 300 nm.

the samples were pre-immersed in nitric acid to dissolve the copper segments. Thus, in the SEM images of the of the array side, one can see the nickel areas separated by voids.

Typical SEM images of the surface and side are shown in Fig. 2. To determine the nanowires diameters D_n and the distance between the long nanowires axes D_{int}, the SEM images of the surfaces were processed using the Statistics2D program [43]. The segment lengths were determined by plotting the intensity profiles along the nanowires on the images of the cleavages. As a result, it was found that the diameter of nanowires, the length of the copper segments, and the periods of the structure are the same for all three samples and are, respectively, $D_n = 50 \pm 6$ nm, $D_{int} = 101 \pm 8$ nm, and $L_{Cu} = 25 \pm 5$ nm. The lengths of nickel segments differ for different samples and are equal to $L_{1Ni} = 145 \pm 5$ nm, $L_{2Ni} = 302 \pm 5$ nm, $L_{3Ni} = 1000 \pm 5$ nm.

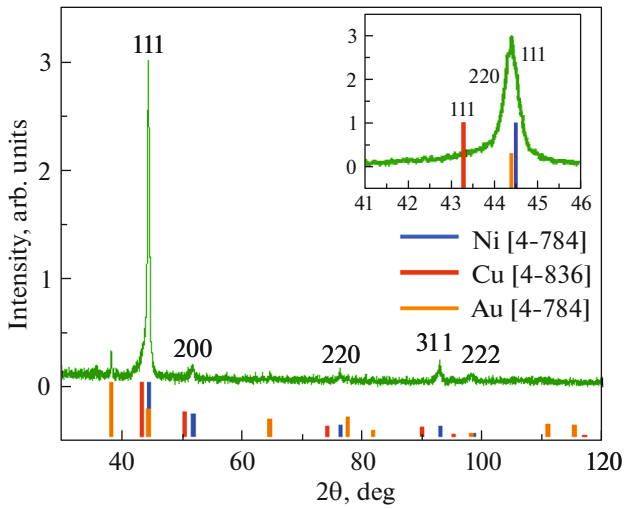

Fig. 3. Diffraction pattern of an array of segmented Ni/Cu nanowires in an AAO matrix.

The atomic structure of the arrays of segmented nanowires was studied using a Rigaku D/MAX 2500 X-ray diffractometer. The measurements were carried out in the Bragg–Brentano (BB) geometry using CuK_α radiation ($\lambda = 1.5418$ Å) in the 2θ range from 30° to 120°.

The main diffraction peaks observed in the X-ray diffraction pattern correspond to Ni (Fig. 3); and there are no oxide phases. Weak peaks of copper, which is much less than nickel, and gold (from the current collector) can also be distinguished. The Ni segments are highly textured, showing a high reflection intensity (111), whereas the intensities of the other peaks are significantly lower. Typically, for a bulk material, the Ni (200) reflection has a relative intensity of 42% (base PC-PDF 2 [4-784]). Taking into account the high reflection intensity (111) and the small line width, it can be concluded that all nickel sections consist of single-crystal large grains oriented mainly in the crystallographic direction ⟨111⟩. It is interesting to note that in the samples with shorter lengths, which were studied in [37], texturing along the ⟨220⟩ direction was found.

3. MAGNETIC PROPERTIES

The measurements of the magnetization reversal curves of arrays of segmented nanowires in AAO matrices were carried out on a QuantumDesign MPMS-5S SQUID magnetometer in the magnetic field range from −20 to 20 kOe with a step from 100 Oe to 1 kOe, depending on the field range at $T = 300$ K.

Figure 4 shows the data obtained by applying a magnetic field parallel and perpendicular to the long

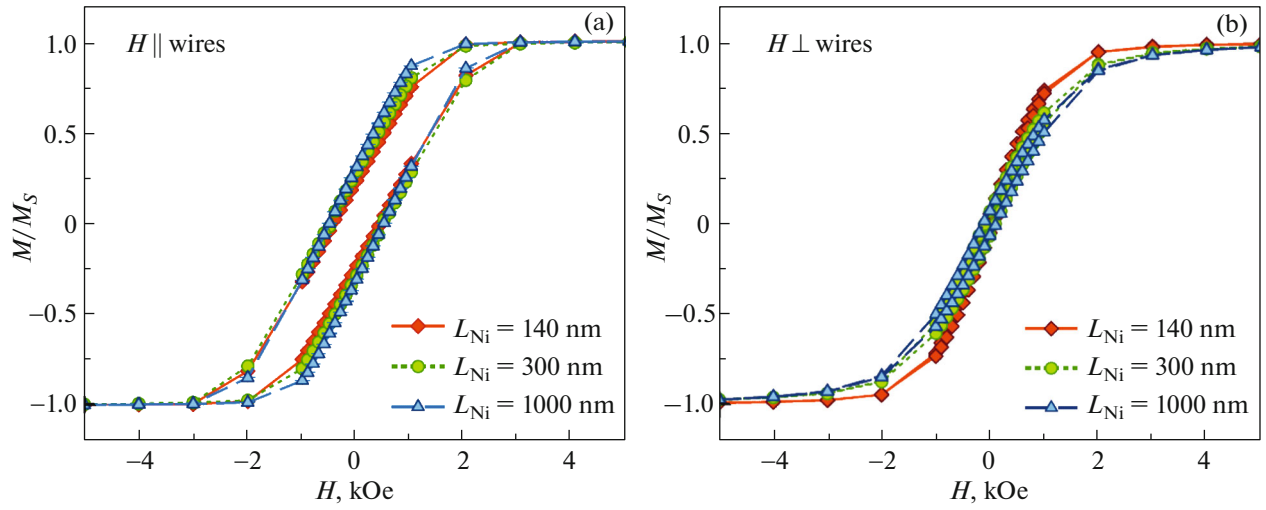

Fig. 4. Curves of magnetization reversal when an external magnetic field is applied along (a) and perpendicular (b) to the long axis of the wires.

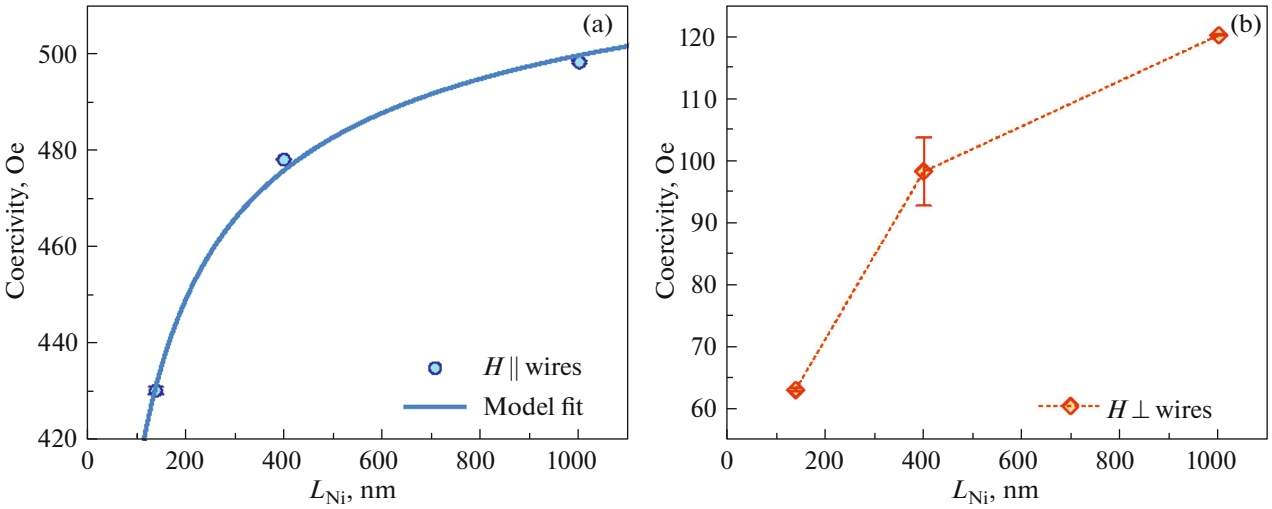

Fig. 5. Dependences of the coercive force on the length of the Ni segment when a field is applied along (a) and perpendicular (b) to the long axis of the wires.

axis of the magnetic nanowires. The curves were normalized to the saturation magnetization value M_S.

It can be seen that the curves differ slightly; however, when the field is applied perpendicular to the axis of the wires, the curve for $L_{1Ni} = 140$ nm stands out from the series. To carry out a more detailed analysis of the magnetic behavior of the studied arrays of nanowires, the following parameters were determined from the magnetization reversal curves: the coercivity, the squareness of the loop (the ratio of the residual magnetization to the saturation magnetization M_R/M_S), and the slope of the curve in the linear section near the zero field.

For both directions of the field, the coercivity increases with the length of the Ni segment. At the same time, there is a sharp increase in the transition from $L_{1Ni} = 140$ nm to $L_{2Ni} = 300$ nm (Fig. 5).

This behavior of the coercivity indicates a decrease in the interaction fields between the nanowires with an increase the length of the Ni segment. To describe this behavior, we used the model of long interacting wires proposed in [44]. In this case, the dependence of the coercivity on the length is described by the expression

$$H_C = H_0\left(1 - \sqrt{\frac{\varepsilon M_S D_n^2}{4H_0 D_{int} L}\left(1 - \frac{1}{\sqrt{1 + \frac{L^2}{D_{int}^2}}}\right)}\right), \qquad (1)$$

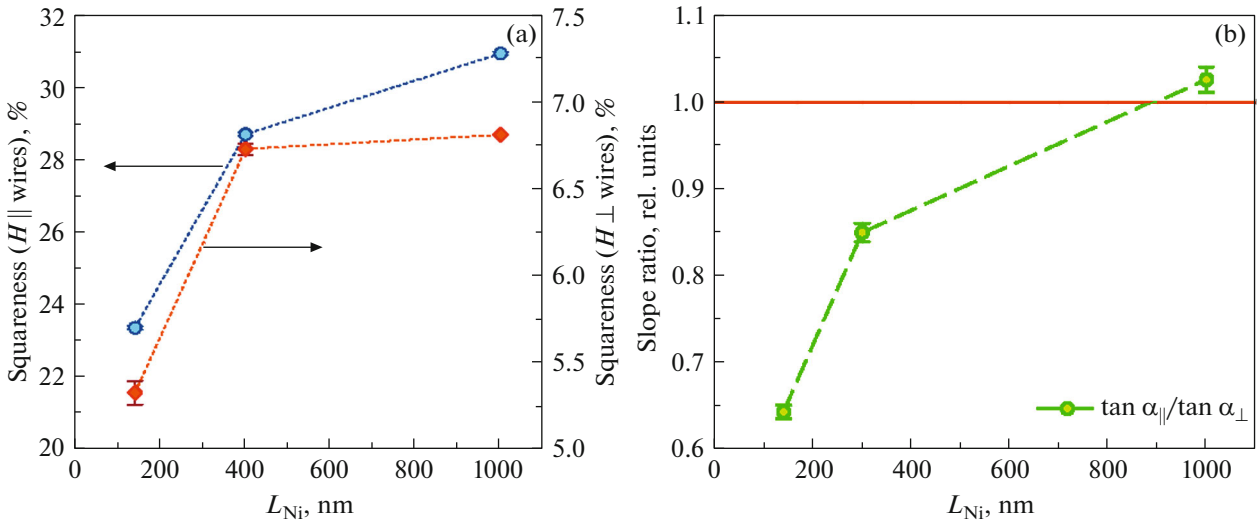

Fig. 6. Dependences of the squareness of the loop on the length of the Ni segment when a field is applied along and perpendicular to the long axis of the wires (a). Dependence of the ratio of the tangents of the slopes of the normalized magnetization reversal curves when a magnetic field is applied along and perpendicular to nanowires on the length of the Ni segment (b).

where H_0 is the coercivity of an infinitely long cylinder, M_S = 6.1 kOe is the saturation magnetization of bulk nickel, ε is an empirical parameter that depends on the mutual arrangement of the wires and takes into account the lowering of the energy barrier during magnetization reversal magnetization [44], D_n = 50 nm and D_{int} = 100 nm.

Figure 5a shows the fitting curve with the following parameters: H_0 = 541 ± 4 Oe, ε = 81 ± 9. It should be noted that in this case, the length of the nickel segment was taken as the independent variable L, and not the total length of the wire.

The chosen model describes the experimental data well; however, if the total wire length rather than the segment length is used as the independent variable L, the same value is obtained for H_0 (this value limits the values of the magnetization reversal field from above and should not change with a change in the scale of the horizontal axis). At the same time, ε increases by a factor of 10 and exceeds the values that have a physical meaning [45, 46]. In addition, the value of the coercivity for a similar array of solid (not segmented) nickel nanowires turns out to be twice as large as H_0 [47].

This behavior can be interpreted as follows: nickel segments interact most strongly with the nearest neighbors located along the same axis, but still do not form a single wire.

The dependences of squareness on the length of the nickel segment are shown in Fig. 6. The nature of the dependence is similar to the behavior of the coercivity. For a field directed perpendicular to the axis of the wires, a sharp jump is also observed at the transition to L_{Ni} = 400 nm, the further change is weakly expressed.

The direction of the external field along the easy magnetization axis corresponds to a lower value of the saturation field with respect to the corresponding value for the direction along the hard magnetization axis. However, the field step in the saturation region in the measurements performed is too large to determine the exact value of the saturation field. However, it can be seen that this value correlates with the slope of the curve in the linear region in the center of the loop, in which there are a large number of measured points. Thus, this angle is, in fact, determined by the magnetization rate.

In this regard, for the analysis of the magnetization anisotropy, the tangent of the slope angle α of the linear sections of the normalized magnetization reversal curves in the range from –1 to 1 kOe was calculated. The ratio of the tangents for the longitudinal and perpendicular directions of the external field was calculated as a parameter that determines the "lightness" of the direction. The results are shown in Fig. 6b.

It can be seen that the ratio of the tangents of the slopes of the magnetization reversal curves in the case of an external field applied parallel and perpendicular to the length of the axis of the wires increases with the length of the nickel segment, and when the L_{Ni} reaches 800—900 nm, it becomes greater than unity. Thus, the direction of the easy magnetization axis changes from perpendicular to the wires to longitudinal. Perhaps this occurs at shorter lengths, but nevertheless at a rather large ratio of wire length to diameter (from 10 to 15). In [37], a similar change occurs up to L_{Ni} = 100 nm, that is, when the ratio of length to diameter is equal to two.

Probably, it is precisely the intersegment interaction within one wire that makes the anisotropy state of

the "easy plane" type (perpendicular to the wires) more favorable than the "easy axis" (parallel to the wires). The overall behavior of the entire array is determined by the balance of interactions between segments within a wire, in adjacent wires, and the contribution of the segment shape anisotropy. Also, the presence of a noticeable texture of nickel grains certainly affects the magnetic characteristics; however, for segments with a high length-to-diameter ratio, this factor plays a lesser role. The number of segments can also have an additional influence, i.e., the total length of the wire, which is of interest for further research.

CONCLUSIONS

In this work, we investigated the magnetic properties of arrays of segmented Ni/Cu nanowires with different lengths of the Ni segment. It was shown that a noticeable change in properties occurs when the length changes from 140 to 300 nm. The character of the dependence of the coercivity on the length of the nickel segments is monotonic and is similar for the directions of the field along and perpendicular to the length of the axis of the wires. It is shown that the direction of the easy magnetization axis changes from perpendicular to the wires to longitudinal. The observed behavior is most likely due to the fact that the interaction between different segments of one wire is greater than between segments of adjacent wires.

ACKNOWLEDGMENTS

The authors are grateful to the management of the Saint Petersburg University Research Park and the employee of the Nanotechnology Research Center (NTRC) (http://nano.spbu.ru) V. D. Kalganov for his inestimable contribution of obtaining experimental data. In addition, the authors are grateful to the developers of the Magic Plot software (https://magicplot.com/), in which most of the graphs are constructed. This work was supported by the Interdisciplinary Scientific and Educational School of Moscow University "The Future of the Planet and Global Environmental Changes."

FUNDING

This work was supported by the Russian Science Foundation (project no. 18-72-00011).

CONFLICT OF INTERESTS

The authors declare that they have no conflicts of interests.

REFERENCES

1. A. O. Adeyeye and N. Singh, J. Phys. D **41**, 153001 (2008).
2. W. Rave, K. Fabian, and A. Hubert, J. Magn. Magn. Mater. **190**, 332 (1998).
3. J.-P. Adam, S. Rohart, J.-P. Jamet, J. Ferre, A. Mougin, R. Weil, H. Bernas, and G. Faini, Phys. Rev. B **85**, 214417 (2012).
4. A. Knittel, M. Franchin, Th. Fischbacher, F. Nasirpouri, S. J. Bending, and H. Fangohr, New J. Phys. **12**, 113048 (2010).
5. R. F. Wang, C. Nisoli, R. S. Freitas, J. Li, W. McConville, B. J. Cooley, M. S. Lund, N. Samarth, C. Leighton, V. H. Crespi, and P. Schiffer, Nature (London, U.K.) **439**, 303 (2006).
6. S. Rajaram, D. K. Karunaratne, S. Sarkar, and S. Bhanja, IEEE Trans. Magn. **49**, 3129 (2013).
7. K. J. Merazzo, D. C. Leitao, E. Jimenez, J. P. Araujo, J. Camarero, R. P. del Real, A. Asenjo, and M. Vazquez, J. Phys. D **44**, 505001 (2011).
8. S. Michea, J. L. Palma, R. Lavin, J. Briones, J. Escrig, J. C. Denardin, and R. L. Rodriguez-Suarez, J. Phys. D **47**, 335001 (2014).
9. C. Donnelly, M. Guizar-Sicairos, V. Scagnoli, M. Holler, Th. Huthwelker, A. Menzel, I. Vartiainen, E. Miiller, E. Kirk, S. Gliga, J. Raabe, and L. J. Heyderman, Phys. Rev. Lett. **114**, 115501 (2015).
10. M. Albrecht, G. Hu, I. L. Guhr, T. C. Ulbrich, J. Boneberg, P. Leiderer, and G. Schatz, Nat. Mater. **4**, 203 (2005).
11. R. Streubel, V. P. Kravchuk, D. D. Sheka, D. Makarov, F. Kronast, O. G. Schmidt, and Yu. Gaididei, Appl. Phys. Lett. **101**, 132419 (2012).
12. A. Fernandez-Pacheco, L. Serrano-Ramon, J. M. Michalik, M. R. Ibarra, J. M. de Teresa, L. O'Brien, D. Petit, D. J. Lee, and R. P. Cowburn, Sci. Rep. **3**, 1492 (2013).
13. A. May, M. Hunt, A. van den Berg, A. Hejazi, and S. Ladak, Commun. Phys. **2**, 1 (2019).
14. K. S. Napolskii, I. A. Sapoletova, D. F. Gorozhankin, A. A. Eliseev, D. Yu. Chernyshov, D. V. Byelov, N. A. Grigoryeva, A. A. Mistonov, W. G. Bouwman, and K. O. Kvashnina, Langmuir **26**, 2346 (2010).
15. I. S. Dubitskii, N. A. Grigoryeva, A. A. Mistonov, G. A. Valkovskiy, N. A. Sapoletova, and S. V. Grigoriev, Phys. Solid State **59**, 2464 (2017).
16. I. S. Dubitskiy, A. V. Syromyatnikov, N. A. Grigoryeva, A. A. Mistonov, A. Sapoletova, and S. V. Grigoriev, J. Magn. Magn. Mater. **441**, 609 (2017).
17. A. A. Mistonov, I. S. Dubitskiy, I. S. Shishkin, N. A. Grigoryeva, A. Heinemann, N. A. Sapoletova, G. A. Valkovskiy, and S. V. Grigoriev, J. Magn. Magn. Mater. **477**, 99 (2019).
18. M. Okuda, T. Schwarze, J. C. Eloi, S. E. W. Jones, P. J. Heard, A. Sarna, E. Ahmad, V. V. Kruglyak, D. Grundler, and W. Schwarzacher, Nanotechnology **28**, 155301 (2017).
19. Ju. Brunner, I. A. Baburin, S. Sturm, K. Kvashnina, A. Rossberg, T. Pietsch, S. Andreev, E. Sturm, and H. Colfen, Adv. Mater. Interfaces **4**, 1600431 (2017).
20. Ch. Phatak, Yu. Liu, E. B. Gulsoy, D. Schmidt, E. Franke-Schubert, and A. Petford-Long, Nano Lett. **14**, 759 (2014).
21. H. Masuda and K. Fukuda, Science (Washington, DC, U. S.) **268**, 1466 (1995).

22. M. Vazquez, *Magnetic Nano-and Microwires: Design, Synthesis, Properties and Applications* (Woodhead, Cambridge, 2020).
23. M. Stano and O. Fruchart, Handbook Magn. Mater. **27**, 155 (2018).
24. P. W. Egolf, N. Shamsudhin, S. Pane, D. Vuarnoz, J. Pokki, A. G. Pawlowski, P. Tsague, B. de Marco, W. Bovy, S. Tucev, M. H. D. Ansari, and B. J. Nelson, J. Appl. Phys. **120**, 064304 (2016).
25. S. Leulmi, X. Chauchet, M. Morcrette, G. Ortiz, H. Joisten, Ph. Sabon, Th. Livache, Ya. Hou, M. Carriere, St. Lequien, and B. Dieny, Nanoscale **7**, 15904 (2015).
26. J. A. Otalora, M. Yan, H. Schultheiss, R. Hertel, and A. Kakay, Phys. Rev. B **95**, 184415 (2017).
27. Zh. Li, M. Wang, Ya. Nie, D. Wang, Q. Xia, W. Tang, Zh. Zeng, and G. Guo, J. Magn. Magn. Mater. **414**, 49 (2016).
28. K. Gandha, K. Elkins, N. Poudyal, X. Liu, and J. P. Liu, Sci. Rep. **4**, 1 (2014).
29. A. Winkler, M. S. Menzel, R. Kozhuharova-Koseva, S. Hampel, A. Leonhardt, and B. Bochner, J. Appl. Phys. **99**, 104905 (2006).
30. N. Maleak, P. Potpattanapol, N. N. Bao, J. Ding, W. Wongkokuo, I. M. Tang, and S. Thongmee, J. Magn. Magn. Mater. **354**, 262 (2014).
31. C. Bran, E. Berganza, J. A. Fernandez-Roldan, E. M. Palmero, J. Meier, E. Calle, M. Jaafar, M. Foerster, L. Aballe, and R. A. Fraile, ACS Nano **12**, 5932 (2018).
32. Ph. Sergelius, J. H. Lee, O. Fruchart, M. S. Salem, S. Allende, R. A. Escobar, J. Gooth, R. Zierold, J.-Ch. Toussaint, S. Schneider, D. Pohl, B. Rellinghaus, S. Martin, J. Garcia, H. Reith, et al., Nanotechnology **28**, 065709 (2017).
33. A. J. Grutter, K. L. Krycka, E. V. Tartakovskaya, J. A. Borchers, K. S. M. Reddy, E. Ortega, A. Ponce, and B. J. H. Stadler, ACS Nano **11**, 8311 (2017).
34. D. Wolf, N. Biziere, S. Sturm, D. Reyes, T. Wade, T. Niermann, J. Krehl, B. Warot-Fonrose, B. Blichner, and E. Snoeck, Commun. Phys. **2**, 87 (2019).
35. S. Moraes, D. Navas, F. Beron, M. P. Proenca, K. R. Pirota, C. T. Sousa, and J. P. Araujo, Nanomaterials **8**, 490 (2018).
36. A. Nunez, L. Perez, M. Abuin, J. P. Araujo, and M. P. Proenca, J. Phys. D **50**, 155003 (2017).
37. M. Susano, M. P. Proenca, S. Moraes, C. T. Sousa, and J. P. Araujo, Nanotechnology **27**, 335301 (2016).
38. A. D. Davydov and V. M. Volgin, Russ. J. Electrochem. **52**, 806 (2016).
39. A. H. A. Elmekawy, E. G. Iashina, I. S. Dubitskiy, S. V. Sotnichuk, I. V. Boshev, K. S. Napolskii, D. Menzel, and A. A. Mistonov, Mater. Today Commun. **25**, 101609 (2020).
40. I. S. Dubitskiy, A. H. A. Elmekawy, E. G. Iashina, S. V. Sotnichuk, K. S. Napolskii, D. Menzel, and A. A. Mistonov, J. Supercond. Nov. Magn. **34**, 539 (2021).
41. K. S. Napolskii, I. V. Roslyakov, A. A. Eliseev, D. I. Petukhov, A. V. Lukashin, S. F. Chen, C. P. Liu, and G. A. Tsirlina, Electrochim. Acta **56**, 2378 (2011).
42. K. S. Napol'skii, I. V. Roslyakov, A. A. Eliseev, A. V. Lukashin, and Yu. D. Tret'yakov, Al'tern. Energet. Ekol., No. 8, 79 (2010).
43. I. V. Roslyakov, D. S. Koshkodaev, A. A. Eliseev, D. Hermida-Merino, V. K. Ivanov, A. V. Petukhov, and K. S. Napolskii, J. Phys. Chem. C **121**, 27511 (2017).
44. S. L. Lim, F. Xu, N. N. Phuoc, and C. K. Ong, J. Alloys Compd. **505**, 609 (2010).
45. P. Allia, M. Coisson, P. Tiberto, F. Vinai, M. Knobel, M. Novak, and W. Nunes, Phys. Rev. B **64**, 144420 (2001).
46. J. Escrig, R. Lavin, J. Palma, J. Denardin, D. Altbir, A. Cortes, and H. Gomez, Nanotechnology **19**, 075713 (2008).
47. R. Lavin, J. Denardin, J. Escrig, D. Altbir, A. Cortes, and H. Gomez, J. Appl. Phys. **106**, 103903 (2009).

Translated by V. Selikhanovich